3D Inversion of Time-Domain Electromagnetic Data for Ground Water Aquifers*

Elliot M. Holtham[1], Mike McMillan[1], and Eldad Haber[2]

Search and Discovery Article #41610 (2015)
Posted April 13, 2015

*Adapted from extended abstract prepared in conjunction with an oral presentation given at the 2014 GeoConvention, Calgary, Alberta, Canada, May 12-16, 2014,

[1]Computational Geosciences Inc., Vancouver, British Columbia (info@compgeoinc.com)
[2]University of British Columbia, Vancouver, BC

Summary

Airborne time-domain electromagnetic surveys are effective tools for ground water aquifer mapping, mineral exploration, and environmental applications. 3D inversion of airborne electromagnetic data is a challenging computational problem. The size of the surveys and the spatial resolution required to adequately discretize the transmitters and receivers result in very large meshes. Solving the forward problem repeatedly on such a mesh can quickly become impractical. Fortunately, using a single mesh for both the forward and inverse problem for all of the transmitters is not necessary. The forward problem for a single source or a small group of sources can be solved on different meshes, each of which need only be locally refined with fine cells close to the selected transmitters and receivers. Away from the selected transmitters and receivers, the mesh can be coarsened. The forward problem can then be broken into a number of highly parallel problems. Each forward modelling mesh is optimized specifically to the selected transmitters and receivers and has far fewer cells than the fine inversion mesh. In this article we present an implementation of this idea, using a finite volume discretization on OcTree meshes. We demonstrate our approach to invert 3D airborne electromagnetic data, and show how it can be used to map ground water aquifers and shale units from aSkyTEM dataset over the Horn River Basin, British Columbia.

Introduction

Airborne electromagnetic (AEM) surveys are economical ways to map water aquifers and geology over large regions. Traditionally, the data from such surveys have been interpreted using time constant analysis, conductivity to depth imaging (CDI), or possibly 1D inversion. These methods assist in a simple interpretation of the data; however, because they do not fully model the physics in 3D, they can fail to accurately represent environments such as real world structures and geological targets. Furthermore, it is difficult to incorporate and constrain 1D inversions based on borehole measurements. Airborne EM datasets are characterized by large volumes of data, as each EM sounding implies a new transmitter location. As a result, inverting this data in 3D is a computationally difficult problem that until recently has not been possible to resolve adequately for the exploration community.

The AEM inverse problem (for example Haber et al., 2007;Cox and Zhdanov, 2008) constitutes finding the spatial distribution of subsurface electrical resistivity which explains the observed data within the limits of the measurement uncertainties. To find such an earth model, one must solve the forward problem, the computation of the predicted data given a resistivity model. When solving the forward problem for AEM surveys, one faces a number of challenges. The first is the significant number of source locations. Controlled source airborne systems consist of a single moving transmitter and receiver that are flown across the survey area by an aircraft. Typical airborne systems record a new sounding every few metres. For airborne surveys where hundreds to tens of thousands of line kilometres of data are collected, a new sounding every few metres can result in thousands to millions of distinct source locations. Typically, the time to solve the forward problem scales linearly with the number of sources; therefore, it is critical that the forward problem is solved very efficiently. The second difficulty is a problem of scales. AEM surveys can cover large areas and aim at resolving both small-and large-scale variations of the subsurface resistivity. To this end, we introduce a mesh which divides the subsurface into cells and we seek to find the resistivity value in each cell. The mesh needs to cover the whole survey area to consistently account for large-scale features that may influence the data even at a considerable distance from the transmitter location. At the same time, the mesh cell size needs to be fine enough to recover the small-scale features and to reflect the spatial resolution of the data. This easily leads to meshes with millions of cells.

Here, we present the implementation of an inversion algorithm which uses a globally fine mesh to solve the inverse problem and a number of locally fine meshes to solve the forward problem for selected transmitter–receiver pairs. This work extends our previous work on time domain electromagnetics inversion using a single regular mesh (Haber et al., 2007) to OcTree meshes. The underlying regular structure of OcTree meshes greatly simplifies mesh handling and algorithmic development, compared to the finite element method on unstructured tetrahedral meshes (Günther, Rücker, and Spitzer, 2006; Schwarzbach et al., 2011). A similar approach has been published by Cox and Zhdanov (2008). While Cox and Zhdanov (2008) first demonstrated the use of footprint-based approaches to solve the forward problems arising from AEM data, we discretize the whole domain and refine the cells far from the transmitters to be coarse. Our approach offers the flexibility to adjust the cell size; it can handle large conductors which can influence the measurement even from a great distance.

Method

We formulate the forward problem as an initial boundary value problem in terms of the magnetic field Hi(x,t),

$$\nabla \times \left(\rho(\mathrm{x}) \nabla \times \mathbf{H}_{\mathrm{i}}(\mathrm{x},\mathrm{t}) \right) + \mu(x) \partial t \boldsymbol{H}_{\mathrm{i}}(x,t) = \nabla \times \left(\rho(x) \nabla \times \boldsymbol{H}_{\mathrm{i}0}(x) f(t) \right) \qquad (1)$$

For x ϵ Ω and t ϵ (0,T]. The initial conditions are given as

$$\boldsymbol{H}_i(x,0) = \boldsymbol{H}_{i,0}(x) \quad (2)$$

and the boundary conditions are

$$\boldsymbol{n} \times (\rho(x) \nabla \times \boldsymbol{H}_i(x,t)) = \boldsymbol{0} \quad (3)$$

Here ρ is the electrical resistivity and μ the magnetic permeability. The subscript i indicates the i^{th} transmitter which we model by a current loop which carries a current f(t). For $t \leq 0$, we assume that $f(t) = I_0$ is constant, giving rise to the magnetostatic field $H_{i,0}(x)$ which satisfies

$$\nabla \cdot \left(\mu(x)\boldsymbol{H}_{i,0}(x)\right) = 0 \quad (4)$$

We discretize the initial boundary value problem (1) in space using the finite volume method on OcTree meshes (Haber and Heldmann, 2007; Horesh and Haber, 2011) and in time using the backward Euler method. This yields a system of linear equations which can be written in compact form as

$$A_i(\boldsymbol{m})u_i = b_i(\boldsymbol{m}) \quad (5)$$

In a standard AEM survey, the time derivative of the vertical magnetic induction ∂Bz/∂t is measured. By denoting $d_{i,j}^{obs}$ the observed value of ∂Bz/∂t at the i^{th} transmitter location, and the j^{th} time channel, the predicted data can be computed from u_i by finite differencing in time, and interpolating in space and time. For time channel j and source-receiver pair i, we have

$$d_{i,j}(\boldsymbol{m}) = \boldsymbol{q}_{i,j}^T \boldsymbol{u}_i = \boldsymbol{q}_{i,j}^T [\boldsymbol{A}_i(\boldsymbol{m})]^{-1} \boldsymbol{b}_i(\boldsymbol{m}) \quad (6)$$

where the vector $\boldsymbol{q}_{i,j}$ contains the interpolation weights and finite difference coefficients. To match the predicted and the observed data, we solve a minimization problem and seek a model vector **m*** such that

$$\boldsymbol{m}^* = \text{argmin } \phi(\mathbf{m}) \quad (9)$$

where , $\phi(\mathbf{m}) = \phi_d + \alpha R(\mathbf{m})$, and the data misfit

$$\phi_d(\mathbf{m}) = \sum_{i=1}^{n_s} \sum_{j=1}^{n_t} \frac{(d_{i,j}(\mathbf{m}) - d_{i,j}^{obs})^2}{(d_{i,j}^{std})^2} \quad (10)$$

n_s denotes the number of sources, n_t the number of measured time channels, $d_{i,j}^{std}$ the standard deviation of the datum $d_{i,j}^{obs}$, α the regularization parameter and R(**m**) a smoothness regularization functional. To minimize the non-linear objection function ϕ(**m**) we use the non-linear least squares method and reduce the data misfit until we reach the target data misfit.

Example

From Petrel Robertson Consulting Ltd. Phase II Report, Devonian shales in the Horn River Basin in northeastern British Columbia host one of the largest shale gas plays in North America. The huge demand for both water sources and sinks has made the identification and characterization of subsurface aquifers a top priority for those looking to develop the shale gas resource in the Horn River Basin (PRCL, 2011). Figure 1 shows a stratigraphic cross-section of the Horn River Basin with the near-surface Quaternary channel aquifers. In October 2008, Geoscience BC started the Horn River Basin Aquifer Project with the goal of understanding the hydro-geologic conditions in the area, to investigate potential aquifers in the Horn River Basin, and to quantify and map reservoir capacity and productivity potential. In 2011 the second phase of the project commenced with the goal of continuing the collection and integration of data from deep saline aquifers (PRCL, 2011), as well as examining the use of airborne electromagnetic data to map near-surface groundwater. In April 2011 SkyTEM completed AEM data acquisition over 4 blocks (Stone Mountain - Block 1, Quicksilver - Block 2, EOG - Block 3, Imperial - Block 4). In total over 2400 line-km of AEM and magnetics data were collected using 200 m line spacing. Figure 2 shows the location of the Horn River Basin project and an example of the SkyTEM high moment Z component data. The data over the Imperial block were inverted in 3D, and Figure 3 shows the 3D resistivity model with a restive cutoff only to show the cells that are less resistive than 15 Ωm. Several interesting conductive features linked to groundwater aquifers are imaged. The inversion result identifies regions 1 and 2 as shown on Figure 3 as potential Quaternary channel aquifers. Region 3 is interpreted as the conductive Buckinghorse Shale unit.

Conclusions

Airborne time-domain electromagnetic (AEM) surveys have been shown to be an effective tool for ground-water aquifer imaging. The data are difficult to invert in 3D because of the number of sources and the size and scales of the computational domain. In this abstract we have proposed a new method to invert large-scale AEM datasets which partitions the forward problem into multiple meshes. Each mesh spans the full computational domain but uses fine mesh cells around the selected transmitters and receivers. This mesh refinement methodology results in a forward modelling mesh that has far fewer cells than the full inversion mesh. Since the forward modelling operation is the bottleneck for AEM inversions, this procedure results in a highly parallel algorithm that can handle arbitrarily large datasets and can deal with many scales of detail in the data. We applied our algorithm to a SkyTEM field dataset from the Horn River Basin in British Columbia. The inversion result maps several interesting potential ground water aquifers as well as the conductive Buckinghorse Shale unit.

References Cited

Cox, L.H., and M.S. Zhdanov, 2008, Advanced computational methods of rapid and rigorous 3-D inversion of airborne electromagnetic data: Communications in Computational Physics, v. 3/1, p. 160-179.

Günther, T., C. Rücker, and K. Spitzer, 2006, Three dimensional modelling and inversion of dc resistivity data incorporating topography – II. Inversion: Geophysical Journal International, v. 166/2, p. 506-517.

Haber, E., and S. Heldmann, 2007, An OcTree multigrid method for quasi-static Maxwell's equations with highly discontinuous coefficients: Journal of Computational Physics, v. 223, p. 783-796.

Haber, E.,D. Oldenburg, and R. Shektman, 2007, Inversion of time domain 3D electromagnetic data: Geophysical Journal International, v. 132, p. 1324–1335.

Horesh, L., and E. Haber, 2011, A second order discretization of Maxwell's equations in the quasi-static regime on OcTree grids: SIAM Journal on Scientific Computing, v. 33, p. 2805-2822.

Petrel Robertson Consulting Ltd (PRCL), 2010, Horn River Basin Aquifer Characterization Geological Report, Prepared for Horn River Basin Producers Group Geoscience BC, January 2010.

Petrel Robertson Consulting Ltd (PRCL), 2011, Horn River Basin Aquifer Characterization Project Phase 2 Geological Report, Prepared for Horn River Basin Producers Group Geoscience BC, September 2011.

Schwarzbach, C., R.-U. Börner, and K. Spitzer, K., 2011, Three-dimensional adaptive higher order finite element simulation for geo-electromagnetics—a marine CSEM example: Geophysical Journal International, v. 187, p. 63-74.

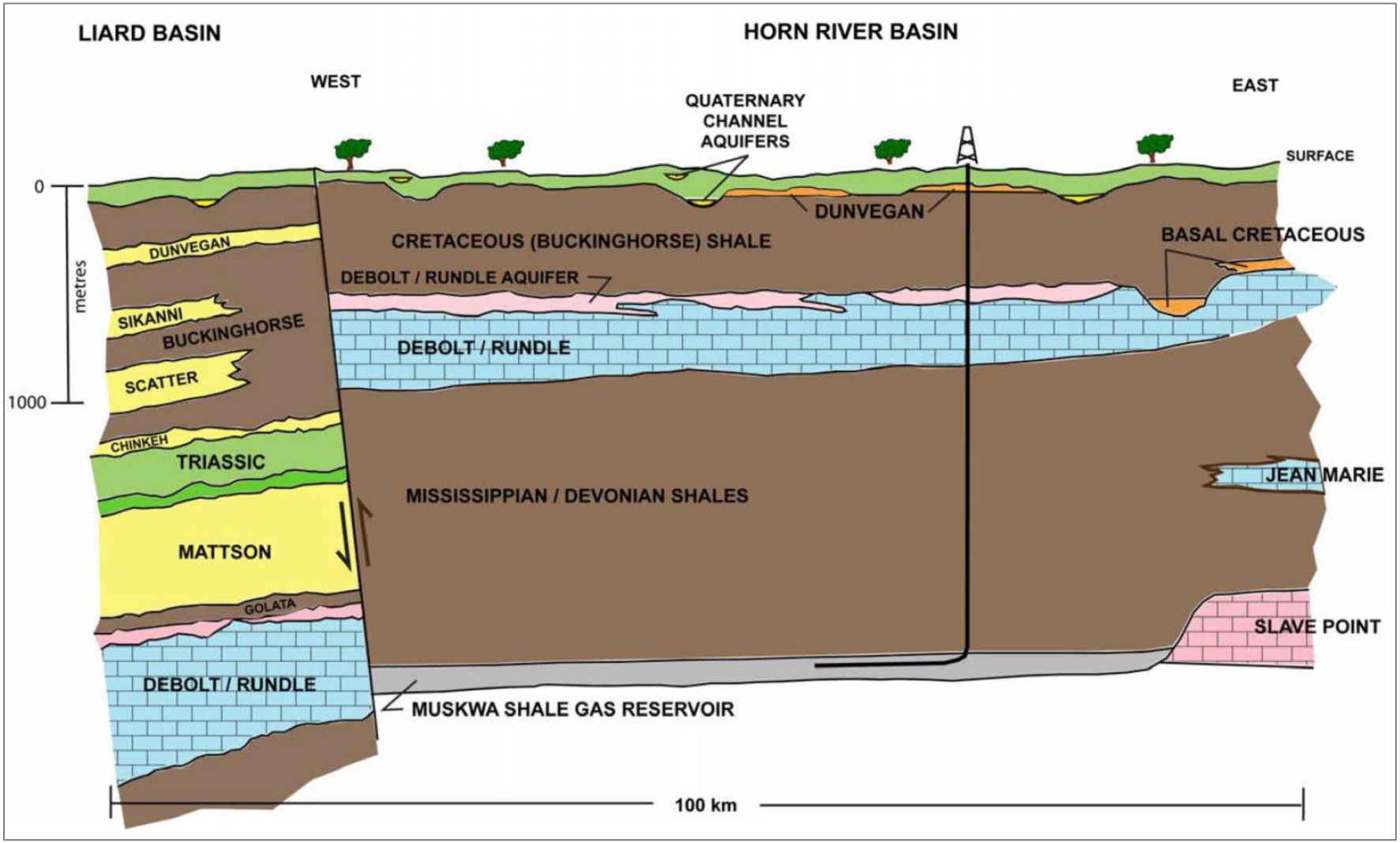

Figure 1. Stratigraphic cross-section of the Horn River Basin and adjacent Liard Basin (from PRCL, 2010).

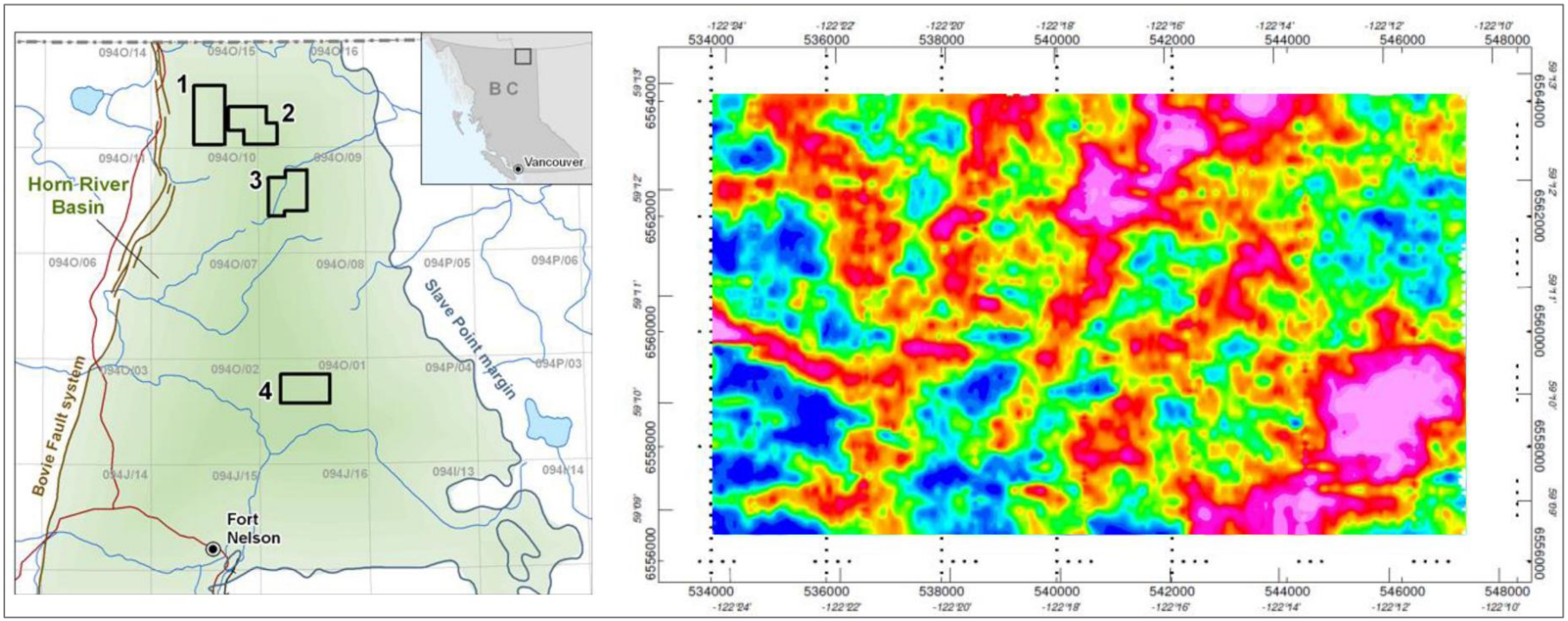

Figure 2. Left: Location of the Horn River AEM blocks. Right: High Moment Z component time gate 12 response (1.79ms) from the Imperial block.

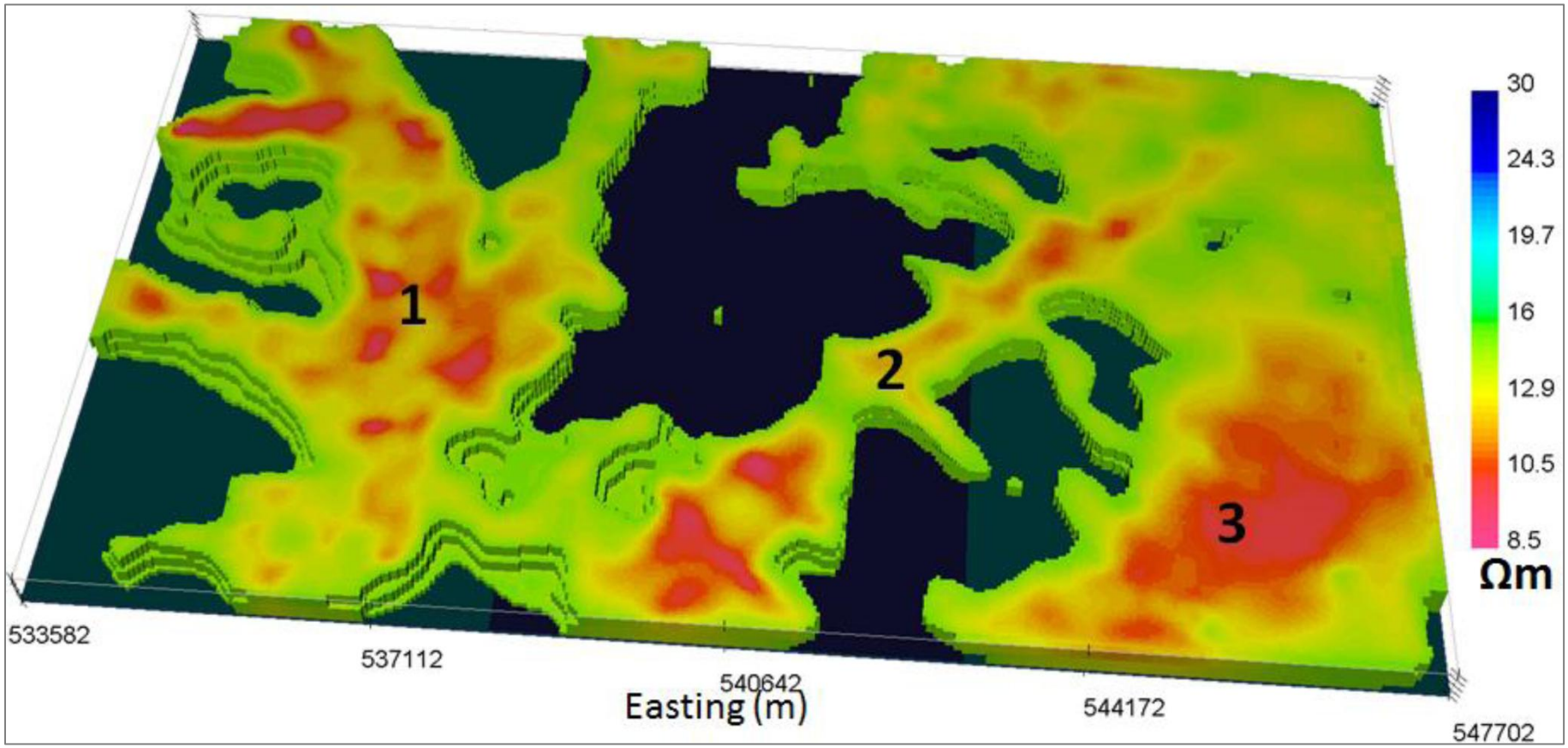

Figure 3. 3D Inversion of SkyTEM data from the Horn River Imperial Block at an elevation of 342 to 292 m above mean sea level (approximately 80 – 130 m below the surface). Regions 1 and 2 are potential Quaternary channel aquifers, and region 3 is likely the conductive Buckinghorse Shale unit.